Basal plane ferromagnetism in the rhombohedral manganite $La_{0.85}Ag_{0.15}MnO_{3+\delta}$

C. B. Larsen, S. Samothrakitis, A. D. Fortes, A. O. Ayas, M. Akyol, A. Ekicibil and M. Laver

Published version information

Citation: C Larsen et al. "Basal plane ferromagnetism in the rhombohedral manganite $La_{0.85}Ag_{0.15}MnO_{3+\delta}$." Journal of Magnetism and Magnetic Materials, vol. 498 (2020): 166192.

DOI: 10.1016/j.jmmm.2019.166192

Basal plane ferromagnetism in the rhombohedral manganite $La_{0.85}Ag_{0.15}MnO_{3+\delta}$

C. B. Larsen[a,b,c], S. Samothrakitis[a,b,c], A. D. Fortes[d], A. O. Ayaş[e], M. Akyol[f], A. Ekicibil[g], M. Laver[h,i]

[a]*School of Metallurgy and Materials, University of Birmingham, Birmingham B15 2TT, United Kingdom*
[b]*Nuclear Physics Institute, Academy of Sciences of the Czech Republic, 25068 Řež near Prague, Czech Republic*
[c]*Institute of Physics, Czech Academy of Sciences, Na Slovance 1992/2, 1822 Prague, Czech Republic*
[d]*ISIS Facility, Rutherford Appleton Laboratory, Harwell Science and Innovation Campus, Didcot, Oxfordshire OX11 0QX, United Kingdom*
[e]*Faculty of Technology, Department of Mechatronics Engineering, Adıyaman University, Adıyaman, Turkey*
[f]*Faculty of Engineering, Department of Materials Engineering, Adana Alparslan Türkeş Science and Technology University, 01250 Adana, Turkey*
[g]*Faculty of Science and Letters, Department of Physics, Çukurova University, 01330 Adana, Turkey*
[h]*School of Physics & Astronomy, University of Birmingham, Birmingham B15 2TT, United Kingdom*
[i]*Department of Physics, University of Warwick, Coventry CV4 7AL, United Kingdom*

Abstract

The structural and magnetic properties of silver-doped lanthanum manganite, $La_{0.85}Ag_{0.15}MnO_{3+\delta}$, $\delta = 0.10(2)$, have been studied using magnetometry and high-resolution neutron powder diffraction. The structural space group is found to be predominantly $R\bar{3}c$, with a minor (5%) fraction of *Pnma* phase. This phase fraction does not change in the measured temperature range of 4 K to 300 K. Our high-resolution diffraction data allow a detailed analysis of the spin orientation. Using representational analysis, we find the ferromagnetic state below $T_c = 246$ K has spins oriented perpendicular to the rhombohedral c-axis and is purely ferromagnetic i.e. no canting between sublattices is observed. Implications for the magnetocaloric effect are discussed.

Keywords: Magnetocaloric effect, Neutron powder diffraction, Manganite

1. Introduction

Perovskite manganites are widely studied due to the striking magnetic phenomena they exhibit, such as the magnetocaloric effect and colossal magnetoresistance. These effects afford huge potential for possible applications in areas such as magnetic refrigeration [1] and magnetic sensors [2]. Both the magnetocaloric effect and colossal magnetoresistance are enhanced in the vicinity of magnetic phase transitions, implying a need for the study of the magnetic structures of candidate materials.

In addition to their budding functional abilities, perovskite manganites also serve as playgrounds for studying strongly correlated electron systems, since their magnetic structures are affected by competing lattice, electronic, spin, and orbital degrees of freedom. The archetypal perovskite manganite is $LaMnO_3$ (LMO), which has been extensively explored by theoretical studies [3, 4, 5] and by experimental methods, including neutron diffraction [6], to elucidate its structural and magnetic properties. LMO possesses an orthorhombic crystal structure (*Pnma*) below the Jahn-Teller (JT) transition of $T_{JT} \approx 750$ K and goes through an A-type antiferromagnetic phase transition at $T_N \approx 140$ K [6]. The MnO_6 octahedra of LMO lie at the heart of the structural and magnetic phenomena. Each Mn ion accommodates four d electrons, with three residing in the t_{2g} orbitals and one in a degenerate e_g orbital. The degeneracy of the e_g orbital can be lifted through a JT-distortion, which couples the magnetic, lattice, electronic, and orbital degrees of freedom [7].

Doping the lanthanum site of LMO with divalent or monovalent ions induces two important changes. The first major effect is the change in valency of some Mn ions from 3+ to 4+ (i.e. from four d electrons to three d electrons) as a result of hole doping. Oxygen ions are able to facilitate double exchange between Mn ions by allowing e_{2g} electrons to hop between MnO_6 octahedra [8, 9]. This then makes a magnetic transition to a ferromagnetic state possible. The actual phase diagrams of mixed valency manganites turn out to be rich, with a number of different realized magnetic structures. For example, the $La_{1-x}Ca_xMnO_3$ compound attains several different magnetic states [10]. At low Ca doping levels its magnetic ground state is a canted antiferromagnet. With increasing Ca doping, this ground state transitions into a charge ordered insulator, a ferromagnetic insulator, a ferromagnetic metallic state, an antiferromagnetic insulator, and finally back into a canted antiferromagnet.

A second doping-induced effect is the structural change caused by altering the average ionic radius at the lanthanum site, r_A. This affects the tolerance factor, $t = (r_A + r_O)/[\sqrt{2}(r_{Mn} + r_O)]$, quantifying the distortion of the perovskite structure [11]. Here r_O and r_{Mn} are the ionic radii of the O and Mn ions. Depending on the size of the dopant ion, doped LMO compounds are often found to crystallize in either the orthorhombic *Pnma* phase, like the parent compound, or in the rhombohedral $R\bar{3}c$ phase [12]. A tolerance factor of $t = 1$ implies an ideal cubic perovskite structure, while lower values indicate some amount of internal strain and, consequently,

Email addresses: larsen@fzu.cz (C. B. Larsen), m.laver@warwick.ac.uk (M. Laver)

buckling of the MnO_6 octahedra [13]. If the ionic radius of the dopant ion is similar to the La ionic radius, as is the case with Ca, the crystal structure will tend towards the *Pnma* phase [14, 15]. However, for larger dopant ions such as Ag, Sr or Ba, the compound will, for high enough concentrations, assume a $R\bar{3}c$ structure [15, 16, 12].

Coexistence of antiferromagnetic and ferromagnetic ordering may be expected given that phase separation and percolation phenomena appear to be an intrinsic feature of manganites [17]. In the non-lanthanum perovskite manganite $Pr_{0.7}Ca_{0.3}MnO_3$, a complex magnetic structure with several propagation vectors and coexisting antiferromagnetic and ferromagnetic phases is observed [12]. Non-trivial propagation vectors have also been observed in the double perovskite multiferroics $TbMn_2O_5$ and $DyMn_2O_5$ [18]. The numerous available magnetic states are not only made possible by the double exchange mechanism but also by the induced changes in the Jahn-Teller distortions of the MnO_6 octahedra due to ionic size mismatches. Changes in the Jahn-Teller distortions affect the Mn-O-Mn bond angles and consequently both the magnetic and structural properties of the doped compound.

Among studied perovskite manganites, compounds doped with monovalent ions, such as Ag^{1+}, have been reported as having promising potential applications [19, 20, 21, 22]. Previous studies of Ag-doped $LaMnO_3$ mostly report a single-phase $R\bar{3}c$ room temperature structure [20, 21], though there is a report of coexisting $R\bar{3}c$ and *Pnma* phases [23]. Differences among reported studies most likely come down to different sample preparation techniques, since the exact oxygen content affects the crystallographic properties of manganites [20]. For instance, at room temperature stoichiometric LMO is found to exhibit a *Pnma* space group, while an excess of oxygen can distort the structure into a $R\bar{3}c$ space group [24]. This structural change occurs due to excess oxygen promoting the oxidation of Mn^{3+} to Mn^{4+} [25]. At room temperature the transition to a rhombohedral space group has been observed to occur at Mn^{4+} concentrations exceeding 21%, corresponding to a stoichiometry of $LaMnO_{3+0.105}$ [25]. The excess oxygen atoms in the nominal LMO formulas are not an indication of interstitial oxygen atoms in the perovskite lattice; rather they have been shown to indicate vacancies on the La and Mn sites [24, 26, 27].

Here we present a magnetometry and neutron powder diffraction study of $La_{0.85}Ag_{0.15}MnO_{3+\delta}$ with the aim of investigating the structural and magnetic phases. In section 2 we describe the experimental methods and results of our magnetization measurements. We identify a ferromagnetic transition at $T_c = 246$ K. The analysis of the neutron diffraction data is presented in section 3. In section 3.1 the structural parameters are resolved via Rietveld refinement by first focusing on the paramagnetic 300 K neutron data, revealing a dominant rhombohedral structure. This structure is seen to persist down to 4 K. The magnetic structure is subsequently resolved in section 3.2, where we determine a transition to a basal plane ferromagnetic structure at T_c.

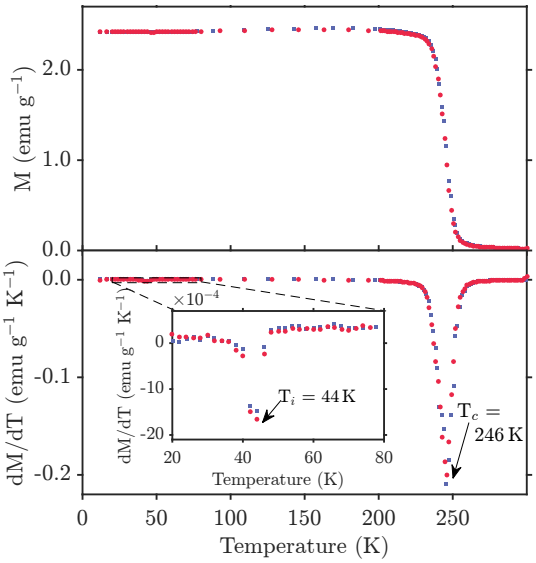

Figure 1: Magnetization measurements on our $La_{0.85}Ag_{0.15}MnO_{3+\delta}$, $\delta = 0.10(2)$, (LAM) powder sample obtained on cooling in an applied magnetic field of 5 mT (blue squares) and subsequently heating the sample back up to 300 K (red circles). The top panel shows the magnetization as a function of temperature. The bottom panel shows the temperature dependence of dM/dT; the inset shows a zoom in of the curve in the low-temperature range.

2. Experimental details

A polycrystalline compound of $La_{0.85}Ag_{0.15}MnO_{3+\delta}$ (LAM) was prepared by a sol-gel method using high-purity powders of La_2O_3, $Mn(NO_3)_2 \cdot 4\ H_2O$ and $AgNO_3$ as starting materials [21, 28], which were mixed and heated at 300°C using a magnetic stirrer. Once precipitation occurred, the solution was heated for 1 hour at 500°C and calcined for 5 hours at 550°C. The compound was then ground using an agate mortar to obtain a fine powder form, then pressed into a disc and sintered at 970°C for 24 hours in air. Further details of the sample preparation can be found in Ref. 28.

Magnetization curves were obtained with a Quantum Design Magnetic Properties Measurement System by applying an external field of 5 mT, field cooling and subsequently warming the sample. The results are shown in Fig. 1, where a transition from a paramagnetic to an ordered state is observed at a temperature of $T_c = 246$ K. We find a magnetic moment of $3.28(4)\,\mu_B$ from a Curie-Weiss fit above the first magnetic transition. Additionally, a second transition is detected at $T_i = 44$ K, where a small kink is observed in each magnetization curve. Similar kinks have been observed in Ag- and Pr-doped LMO compounds, which were interpreted as signs of a transition to an antiferromagnetic phase [21]. Here we find T_i is associated with a Mn_3O_4 impurity phase.

Neutron powder diffraction (NPD) patterns were obtained with the High Resolution Powder Diffractometer (HRPD) at the ISIS spallation neutron source, UK [29]. The neutron data is publicly available [30]. HRPD is a time-of-flight instrument situated on a very long primary flight path (95 m, of which 91.7 m is along a supermirror guide) with fixed detector banks in backscattering (bank 1: $154° < 2\theta < 176°$), orthogonal to

the incident beam (bank 2: $80° < 2\theta < 100°$) and in forward scattering (bank 3: $32° < 2\theta < 28°$). As one would expect, resolution is highest in bank 1, $\Delta d/d \approx 6 \times 10^{-4}$. The instrument uses beam choppers to define a fixed time-of-flight range for measurements; in normal operation, this is 100 ms wide covering the range from 30 – 130 ms, equivalent to a d-spacing range of 0.65 – 2.60 Å in bank 1.

Measurements were carried out with powder samples packed into slab-geometry cans, which allow for accurate and precise temperature control using embedded heater cartridges and RhFe resistance thermometry. These were filled under a helium atmosphere. The front and back faces of the can consist of vanadium-foil windows mounted in a steel frame. The steel frame is sealed with indium wire to the Al-alloy body of the can. All parts of the sample cans, apart from the vanadium windows, were shielded from the incident beam using Gd and Cd foils. Low temperatures were achieved using a He-flow cryostat mounted in the HRPD sample tank.

Data were collected at 4.2 K for 1 hr, followed by warming directly to 300 K and measurement of another 1 hr dataset. The sample was then cooled back to 30 K and a series of shorter runs (30 min) were made in 5 K increments between 30 and 70 K. Raw data were time-focused, normalised to the incident spectrum and corrected for instrument efficiency using the Mantid suite of powder diffraction algorithms [31]. Additionally, a correction was made for the specimen absorption using the known chemical stoichiometry, the sample mass and the specimen geometry, also using Mantid.

Rietveld refinements were performed with the FullProf software package [32]. In the present analysis, both $R\bar{3}c$ (no. 167) and *Pnma* (no. 62) space groups have been included to establish the fractional occurrence of these phases in the sample. This is done due to the known tendency of $La_{0.85}Ag_{0.15}MnO_3$ to crystallize in either space group, or a mixture of both, depending on the exact stoichiometry of the sample [20, 21, 23]. For the $R\bar{3}c$ space group, the hexagonal setting with a general multiplicity of 36 has been used. In the refinement, the peak shapes have been modeled with a convolution of a pseudo-Voigt function and two back-to-back exponentials. This peak shape has also been used for intensity investigations of individual peaks. The default FullProf nuclear and magnetic form factors have been used for the neutron diffraction pattern calculations. A valency of 70:30 has been used for the magnetic Mn^{3+}/Mn^{4+} form factors as expected for the 15% monovalent Ag doping. Special attention is given to the oxygen content of the samples due to the possible implications for the observed structural properties [24, 25]. Possible magnetic structures have been found by performing representational analysis with the SARAh software package [33].

3. Results and discussion

3.1. Structural properties

We proceed by describing the structural properties of our $La_{0.85}Ag_{0.15}MnO_{3+\delta}$ sample. From Rietveld refinements of our 300 K diffraction data (cf. left panels of Fig. 2), we found a majority (95.25(52)%) rhombohedral $R\bar{3}c$ phase along with a minority (4.75(25)%) orthorhombic *Pnma* phase. Detailed $R\bar{3}c$ refinement parameters are listed in Table 1 along with the *Pnma* unit cell parameters. The $R\bar{3}c$ parameters are in rough agreement with those presented for rhombohedral $La_{0.85}Ag_{0.15}MnO_3$ in Ref. 21. Fig. 3 depicts the $R\bar{3}c$ structure. The relative tilting of the MnO_6 octahedra are obvious along the pseudocubic fourfold direction, thus affirming the presence of JT-distortions in the system.

In our analysis we did attempt to fit a monoclinic $P112_1/a$ phase, which was reported to describe the structure of undoped LMO after being heated in air at 1350° for two days [35]. Our best possible fits with this phase to both the 300 K and 4 K patterns gave barely monoclinic structures (i.e. $\gamma - 90° < 0.01°$). Based on this we conclude that such a low-symmetry structure is not warranted for our sample and that the majority rhombohedral phase is more than adequate. A room temperature rhombohedral structure was reported for $La_{1-x}Ag_xMnO_3$ with $x = 0.15$ [21] and also in a separate study for x in the range 0.1–0.2 [20]. However, in Ref. 23 almost equal fractions of $R\bar{3}c$ and *Pnma* phases were found.

Attempts to refine the Ag occupancy turned out to be non-conclusive due to error bars being larger than the possible range of the Ag occupancy parameter. To evince successful Ag doping, the Ag occupancy was manually reduced to 0, which resulted in an increase of the global χ^2 from 3.3 to 6.3. This indicates that some Ag ions did indeed partially-occupy the La site. We refined the oxygen occupation numbers in the 300 K pattern, leading to the fitted stoichiometry of $La_{0.85}Ag_{0.15}MnO_{3.00+0.10(2)}$. According to studies of excess oxygen in LMO [24], this corresponds to a crystallographic structure of $(La_{0.85}Ag_{0.15})_{\delta/(3+\delta)}Mn_{\delta/(3+\delta)}O_3$ = $(La_{0.85}Ag_{0.15})_{0.97(6)}Mn_{0.97(6)}O_3$. Indeed, refining the vacancies of the La and Mn sites, while keeping the occupancy of the oxygen site constant, gave the composition $(La_{0.85}Ag_{0.15})_{0.98(4)}Mn_{0.96(5)}O_3$, which thus agrees with the nominal composition $La_{0.85}Ag_{0.15}MnO_{3.00+0.10(2)}$. From the refinement, the vacancy levels of the La and Mn sites are equal within error bars. Hence it is sufficient to characterize the overall vacancy level of the two sites via a single parameter related to the excess oxygen. This is unlike the two-parameter description employed in Ref. 27.

The extra oxygen atoms could, in conjunction with the assumed 15% Ag doping, mean that the Mn^{3+}:Mn^{4+} ratio is as much as 50:50 in our sample. Unfortunately we find that we are not able to refine the Mn^{3+}:Mn^{4+} ratio e.g. by exploiting the slight difference in q-dependence of their magnetic form factors in our 4 K data. This is because, in the refinement, the Mn^{3+}:Mn^{4+} ratio is coupled to the B_{iso} values and to the neutron absorption correction, due to their similar dependences on q. Indeed the anomalously low B_{iso} values for Mn listed in Table 1 (where we have fixed the Mn^{3+}:Mn^{4+} ratio to 70:30) are likely due to data reduction artefacts such as the numerical correction for the effects of neutron absorption across different detector banks. Fixing the Mn^{3+}:Mn^{4+} ratio to 50:50 instead of 70:30 yields slightly higher χ^2 values of 3.12/7.84/1.54 for banks 1/2/3 for the 4 K data, with the refined Mn B_{iso} value re-

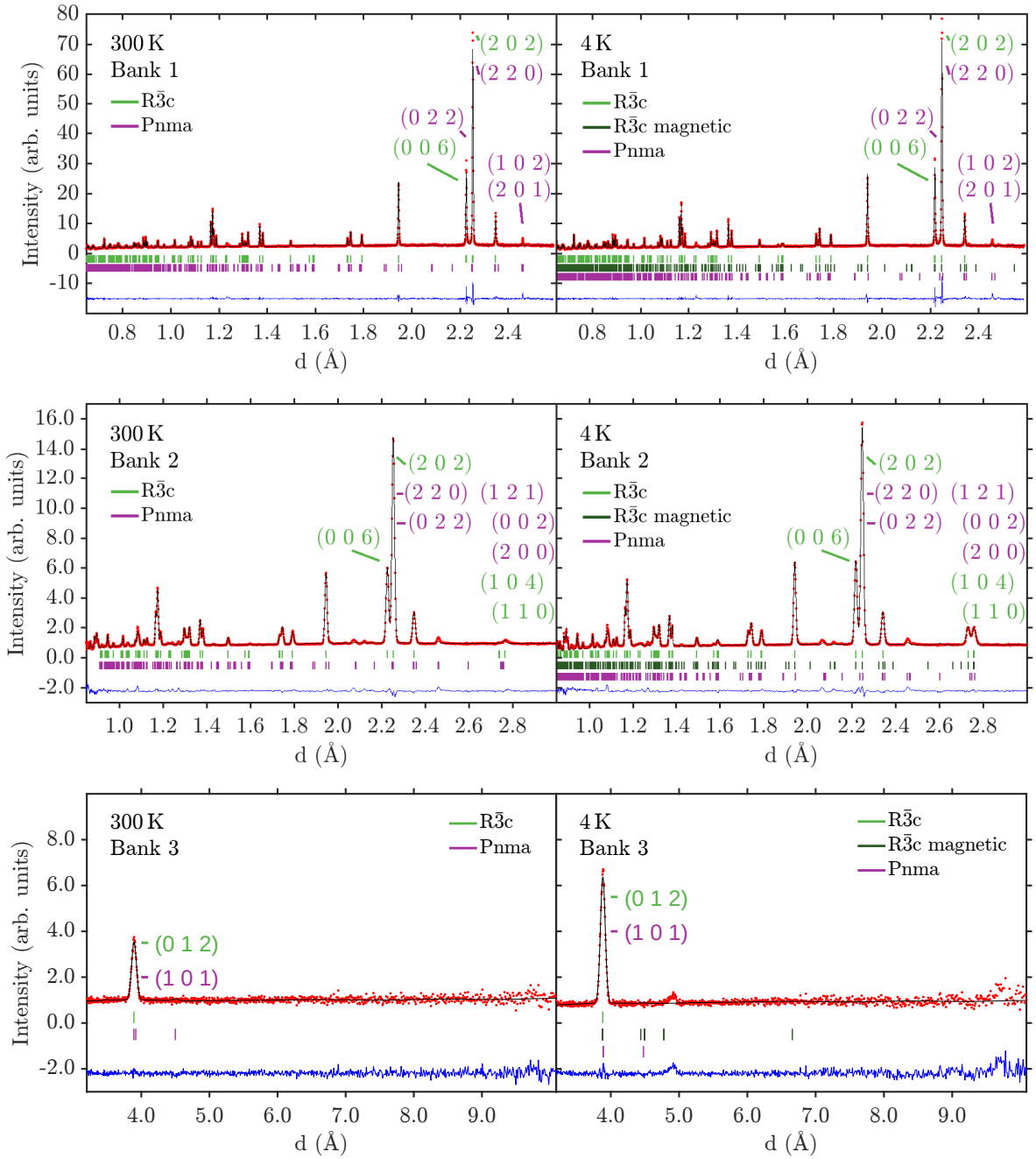

Figure 2: Rietveld refinements of the neutron powder diffraction (NPD) patterns from our $La_{0.85}Ag_{0.15}MnO_{3+\delta}$, $\delta = 0.10(2)$, (LAM) sample at 300 K and 4 K. From top to bottom are shown patterns from detector bank 1, 2, and 3. The red points mark the experimental data, the black line is the refinement, and the blue line displays the residuals. The vertical lines show the positions all the (h k l)-peaks of the space groups in the given range. High-intensity and important peaks have been labeled with (h k l)-indices. The 300 K refinement is purely nuclear and has been carried out with the $R\bar{3}c$ (light green lines) and *Pnma* (magenta lines) space groups, while the 4 K refinement comprises the same structural $R\bar{3}c$ and *Pnma* phases as well as the Γ_5 basal plane ferromagnetic-$R\bar{3}$c phase (dark green lines).

Table 1: Structural and magnetic properties of $La_{0.85}Ag_{0.15}MnO_{3.00+0.10(2)}$ (LAM) obtained from Rietveld refinements of 300 K and 4 K neutron powder diffraction (NPD) patterns. A structural and a magnetic $R\bar{3}c$ phase and a structural *Pnma* phase are refined. Values for the overall refinement parameters are listed in for banks 1/2/3 respectively. For the *Pnma* phase, we do not list the refined atom positions and do not include a magnetic *Pnma* phase due to the small phase fraction. Cell parameters, atom positions, magnetic moment, and the O occupancy are listed for the $R\bar{3}c$ phase. The 6a, 6b, and 18e labels refer to the Wyckoff positions of La/Ag, Mn and O.

	Temperature	
Global parameters	300 K	4 K
χ^2	2.36/6.47/0.99	2.88/7.79/1.43
R_{exp} (%)	9.58/4.11/33.9	8.25/3.40/21.1
R_{wp} (%)	14.7/10.5/33.7	14.0/9.49/25.3
R_p (%)	21.4/15.8/121.0	18.9/14.2/69.5
$R\bar{3}c$ **phase** (%)	95.25(52)	95.02(47)
Pnma **phase** (%)	4.75(25)	4.98(22)
$R\bar{3}c$ **parameters**	300 K	4 K
a (Å)	5.5281(1)	5.5170(2)
c (Å)	13.3590(3)	13.3175(3)
Volume (Å^3)	353.55(1)	351.03(1)
Mn-O-Mn (deg.)	163.89(1)	164.01(4)
Mn-O (Å)	1.9651(1)	1.960(6)
6a: La/Ag (x, y, z)	$\left(0, 0, \frac{1}{4}\right)$	$\left(0, 0, \frac{1}{4}\right)$
6b: Mn (x, y, z)	$\left(0, 0, \frac{1}{2}\right)$	$\left(0, 0, \frac{1}{2}\right)$
18e: O (x, y, z)	$\left(0.4500(2), 0, \frac{1}{4}\right)$	$\left(0.4508(3), 0, \frac{1}{4}\right)$
La/Ag B_{iso} (Å^2)	0.38(3)	0.25(3)
Mn B_{iso} (Å^2)	0.10(5)†	0.01(5)†
O B_{iso} (Å^2)	1.01(2)	0.51(2)
O_{occ}	3.10(2)	-
Mag. Moment (μ_B)	-	3.37(5)
R_M-factor (%)	-	7.31/19.8/0.559
R_B-factor (%)	3.87/5.09/2.74	3.52/5.85/0.559
Rf-factor (%)	5.16/5.92/1.38	3.67/2.11/0.279
Pnma **parameters**	300 K	4 K
a (Å)	5.507(2)	5.523(2)
b (Å)	7.836(3)	7.777(2)
c (Å)	5.494(2)	5.482(2)
Volume (Å^3)	237.1(2)	235.5(1)

†The low Mn B_{iso} values compared to those for the other ions are believed to stem from artefacts in the Rietveld refinement, in particular the correction for the effects of neutron absorption across different detector banks. See text for more details.

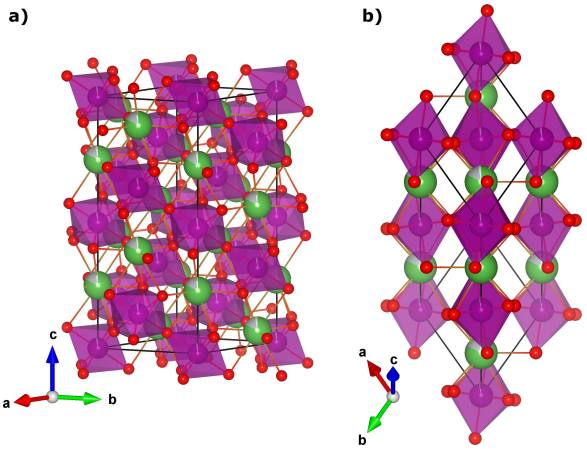

Figure 3: (a) Structural model of the rhombohedral phase of $La_{0.85}Ag_{0.15}MnO_{3+\delta}$ (LAM) at room temperature, with O ions being red, La/Ag ions being green and Mn ions being encapsulated in purple octahedra. The unit cell boundaries are marked with a solid black line. (b) A view of the same rhombohedral LAM structure along a pseudocubic fourfold direction. From this perspective the relative tilting of the octahedra is clear. Both figures have been produced with the *VESTA* visualization program [34].

maining anomalously low at 0.03(4) Å^2. Conversely, fixing the Mn B_{iso} value at a more reasonable 0.27 Å^2 and refining the Mn valency yields a 50:50(20) ratio for Mn^{3+}:Mn^{4+}, also with slightly higher χ^2 values of 2.98/7.94/1.54 for banks 1/2/3.

The Mn valency has some bearing on the observed crystal structure. For example, the Shannon radius of Mn^{4+} is 0.530 Å and is smaller compared to the 0.645 Å radius of Mn^{3+} [36], so a greater fraction of Mn^{4+} will increase the tolerance factor t. The tolerance factors of the parent compound LMO, LAM with a 70:30 Mn^{3+}/Mn^{4+} valency, and LAM with a 50:50 Mn^{3+}:Mn^{4+} valency are calculated to be 0.88, 0.90, and 0.92, respectively. Thus, the Ag doping will help stabilize the perovskite structure.

A quantitative way of substantiating the $R\bar{3}c$ and *Pnma* phase fractions from the Rietveld refinement is to examine the relative intensities and positions of two neighboring peaks and compare them with the calculated phase intensities. This is given in Fig. 4, focusing on the two high intensity peaks in bank 1. As is evident from the 300 K data set, the two experimental peaks are too far apart to be accurately described by purely the *Pnma* phase with the cell parameters given in Table 1, confirming the high percentage of $R\bar{3}c$ found by the Rietveld refinement. A similar structural analysis has been carried out at 4 K. At this temperature, the magnetic contribution, based on the basal plane ferromagnetic magnetic model presented in the next section, is found to only make up $\approx$ 3% of the intensity in the left peak at d = 2.22 Å and $\approx$ 1% of the intensity of the right peak at d = 2.25 Å. Magnetic contributions are therefore ignored in this rough quantification of the structural model. The relative experimental intensity ratio of the left peak with respect to the right peak is found to be 0.37(1) at 300 K, while the corresponding ratio based on the $R\bar{3}c$ pattern calculation of the (0 0 6) and (2 0 2) peaks is 0.39. At 4 K, the experimental relative intensity ratio is found to be 0.38(1) and the pattern

calculation based on the purely structural $R\bar{3}c$ phase, with no magnetic contributions, is found to be 0.37. Thus, the phase ratio between the phases is expected to remain roughly constant as a function of temperature. Fig. 5 shows the temperature-dependence of the structural properties of LAM extracted from Rietveld refinements at all temperatures. In agreement with our intensity analysis, the phase fraction stays constant within error bars. The unit cell parameter and Mn-O bond length all thermally expand with increasing temperature, while the Mn-O-Mn bond angle decreases.

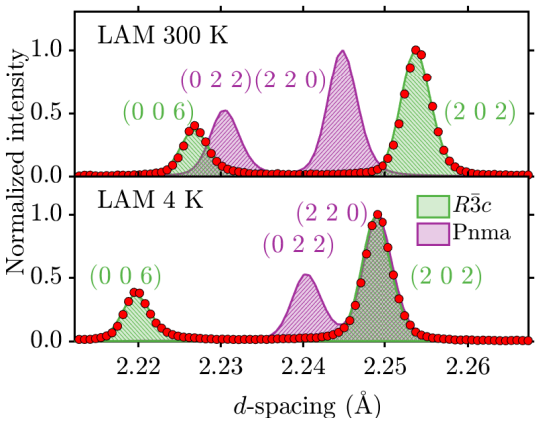

Figure 4: A closer view of the two high-intensity peaks in bank 1. Experimental neutron powder diffraction data at 300 K and 4 K are shown with red circles, while calculated structural phase profiles of a pure $R\bar{3}c$ phase and a pure *Pnma* phase are depicted by shaded green and purple areas, respectively. Both experimental and calculated intensities have been normalized such that the maximal intensity of any data set in the depicted d-range is 1.

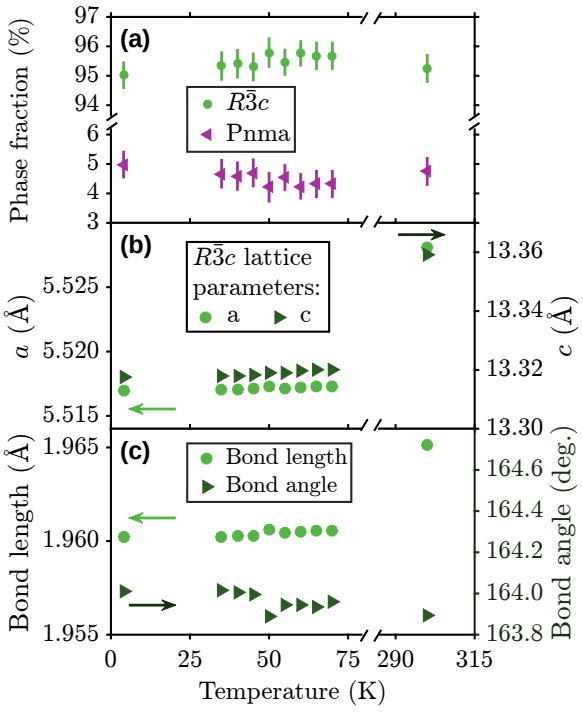

Figure 5: Parameters extracted from Rietveld refinements of powder patterns measured between 4 K and 300 K. (a) Phase fractions of $R\bar{3}c$ and *Pnma*. (b) Cell parameters of the $R\bar{3}c$ phase. (c) The $R\bar{3}c$ Mn-O bond length and Mn-O-Mn bond angle. In (b) and (c) the error bars lie within the symbol size.

3.2. *Magnetic properties*

Our magnetic analysis hinges on the temperature-dependent behaviour of diffraction peak intensities and representational analysis to explore possible magnetic structures. Our LAM sample exhibits two magnetic transitions in the magnetometry data; a ferromagnetic transition at $T_c = 246$ K and another transition at $T_i = 44$ K. From the neutron data, the ferromagnetic nature of the first transition is evident from the lack of new diffraction peaks and an increase in the intensity of low-angle peaks below T_c, while the second transition coincides with the appearance of a new diffraction peak at $d = 4.95$ Å in bank 3. We find that this extra peak and transition temperature are congruent with a Mn_3O_4 impurity phase. Mn_3O_4 has a Curie temperature of 43 K and possesses a tetragonal structure with space group $I4_1/amd$ and room temperature cell parameters of $a = b = 5.763$ Å and $c = 9.546$ Å [36]. The magnetic unit cell is doubled to $(a, 2a, c)$. The extra magnetic peak in bank 3 matches the (0 2 1) magnetic Mn_3O_4 reflection, while a structural peak at $d = 2.46$ Å in bank 1 fits with the (0 4 2) Mn_3O_4 reflection. We calculate the ratio of the experimental intensity of the (0 4 2) Mn_3O_4 peak to the adjacent (1 1 3) $R\bar{3}c$ LAM peak as well as the experimental ratio of the (0 2 1) Mn_3O_4 peak to the (0 1 2) $R\bar{3}c$ LAM. We compare these ratios to theoretical ratios, calculated from the squared $R\bar{3}c$ structure factors as given by FullProf and from the magnetic intensities of the Mn_3O_4 (0 4 2) group of reflections from Ref. 37. With this approach, we estimate an impurity phase fraction of 1.1%.

The Mn ions of the $R\bar{3}c$ phase occupy the 6b high-symmetry site, which limits the orientation of the spins. Possible ferromagnetic structures were established via representational analysis. Using the $R\bar{3}c$ space group, the $\mathbf{k} = (0, 0, 0)$ propagation vector, and the special positions $(0, 0, 0)$ and $\left(0, 0, \frac{1}{2}\right)$ as input parameters, the decomposition of the magnetic structure was found to be $\Gamma_{R\bar{3}c} = 1\Gamma_1 + 0\Gamma_2 + 1\Gamma_3 + 0\Gamma_4 + 2\Gamma_5 + 0\Gamma_6$, where the non-trivial irreducible representations are given in Table 2. This decomposition is the same used to characterize the magnetic structure of Ca_3LiOsO_6, which exhibits the same space group symmetry but a different, double perovskite, unit cell [38]. Similarly, it has been used to characterize the magnetic structure of off-stoichiometric rhombohedral LMO [39]. According to the decomposition, three different magnetic irreducible representations are allowed; Γ_1 corresponds to an A-type antiferromagnetic phase with spins aligned along the c-direction, Γ_3 a ferromagnetic phase with spins aligned along the c-direction, and Γ_5 a ferromagnetic phase with spins aligned perpendicular to the c-axis. Because of the second order nature of the phase transition at $T_c = 246$ K of our magnetization data (c.f. Fig. 1), the magnetic structure should be described by a single irreducible representation.

To decide which of the three possible irreducible representations is compatible with the LAM magnetic structure, the intensities of specific experimental magnetic peaks are compared

Table 2: Basis vectors of the irreducible representations (IR) of a commensurate magnetic order of $R\bar{3}c$, found via representational analysis with a propagation vector of $\mathbf{k} = (0, 0, 0)$ and Mn atoms at the (0,0,0) and (0,0,1/2) special positions.

IR	Basis vector	Atom position	m_a	m_b	m_c
Γ_1	ψ_1	(0,0,0)	0	0	1
		(0,0,1/2)	0	0	-1
Γ_3	ψ_2	(0,0,0)	0	0	1
		(0,0,1/2)	0	0	1
Γ_5	ψ_3	(0,0,0)	1	0	0
		(0,0,1/2)	0	0	0
	ψ_4	(0,0,0)	0	0	0
		(0,0,1/2)	-1	-1	0
	ψ_5	(0,0,0)	0	0	0
		(0,0,1/2)	-1	1	0
	ψ_6	(0,0,0)	-1	-1	0
		(0,0,1/2)	0	0	0

with the calculated profiles. The two peaks positioned closely together at $d = 2.73$ Å and $d = 2.76$ Å in bank 2 are essential to the magnetic analysis, because the peaks show a clear temperature dependence and appear in a detector bank that has both a relatively high resolution and many concurrent structural peaks. The fact that they are closely placed together means that their *relative* intensity can be compared without needing to account for the q-dependence of the magnetic form factor. The two peaks are from left to right indexed as (1 0 4) and (1 1 0) in the $R\bar{3}c$ phase. Since neutrons only scatter from spin components that are perpendicular to the scattering vector $\mathbf{q}$, these two reflections enable us to distinguish between different irreducible representations. For example, the ferromagnetic Γ_3 structure will contribute more intensity to the (1 1 0) peak than to the (1 0 4) peak, because the (1 1 0) peak is fully perpendicular to the c-axis.

The rhombohedral (1 0 4) and (1 1 0) peaks in the experimental data at 4 K are of roughly equal intensity, having a relative ratio of $I(d = 2.73\,\text{Å})/I(d = 2.76\,\text{Å}) = 0.9(1)$, as based on two Gaussian fits to the peaks. The experimental data, along with calculated patterns with purely structural and purely magnetic contributions, are shown in Fig. 6. The same fixed scale factor is used for all the peaks and have been determined from a full refinement to all of the peaks in bank 2. It is evident that the Γ_3 structure contributes more intensity to (1 1 0), the antiferromagnetic Γ_1 structure contributes no intensity to either peak, and the Γ_5 structure contributes more intensity to the (1 0 4) peak. Since the structural $R\bar{3}c$ phase contributes more intensity to the (1 1 0) peak, the Γ_5 structure is the most likely magnetic phase candidate. This is confirmed by the calculated pattern ratios from the different irreducible representations. The phase contribution from the purely structural $R\bar{3}c$ phase strongly favors the right peak, as evidenced from a calculated pattern ratio of $I(d = 2.73\,\text{Å})/I(d = 2.76\,\text{Å}) = 0.06$. The same is true of the purely structural *Pnma* phase, where the same ratio was calculated to be 0.08. A purely $R\bar{3}c$-ferromagnetic Γ_3 phase gives a ratio of 0.31, while a purely $R\bar{3}c$-ferromagnetic Γ_5 phase gives a ratio of 1.59. For a mixed structural phase with 95.02% $R\bar{3}c$ and 4.98% *Pnma* combined with a $R\bar{3}c$-ferromagnetic Γ_3 phase, one

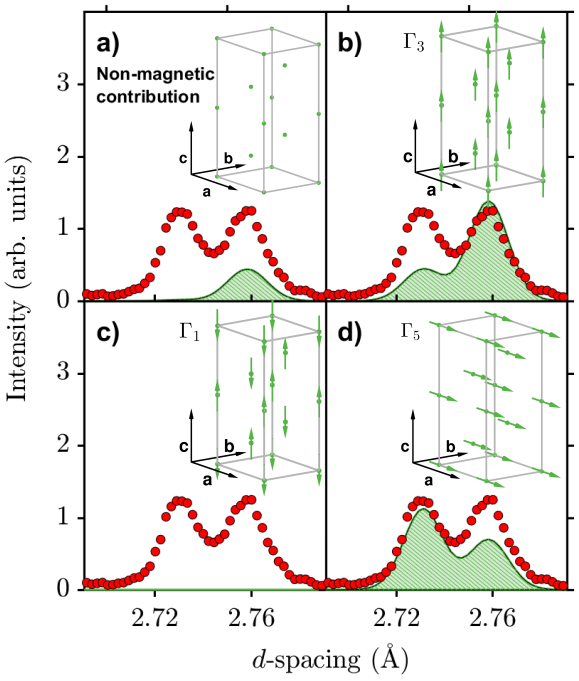

Figure 6: Characterization of the strong rhombohedral (1 0 4) and (1 1 0) peaks in bank 2 of the $La_{0.85}Ag_{0.15}MnO_{3+\delta}$, $\delta = 0.10(2)$, (LAM) neutron powder data. The red points are the experimental data, and the green areas are the calculated profiles based on the (a) non-magnetic structural $R\bar{3}$c contribution, (b) Γ_3 ferromagnetic phase, (c) Γ_1 A-type antiferromagnetic phase, and (d) a Γ_5 basal plane ferromagnetic phase. The magnetic pattern calculations were performed with a magnetic moment at the Mn site of $3.3\,\mu_B$.

obtains a ratio of 0.24. A similar calculation with the Γ_3 phase replaced by a Γ_5 phase results in a ratio of 0.97. Thus, the use of the Γ_5 irreducible representations results in the best agreement between the pattern calculation and the experimental data.

In the Γ_5 irreducible representation, spins can be oriented along any direction in the *ab*-plane. Because the two axes are equivalent in the $R\bar{3}c$ phase, the spins have been arbitrarily chosen to lie along the b axis. Attempts to rotate the spins in other directions did not change the χ^2. An additional attempt to change the angle between spins located at different special positions has also been made. However, any angle above 0° results in intensity contributions to the rhombohedral (0 1 1) peak at $d = 4.50$ Å in bank 3, which has no measurable intensity in our experimental data. This therefore indicates a fully ferromagnetic structure oriented in the *ab*-plane, which differs from the magnetic structure of rhombohedral $LaMnO_{3+0.15}$ determined by Alonso *et al.* in Ref. 39. In this study, a basal plane ferromagnetic Γ_5 magnetic structure was also found to be most compatible with the neutron diffraction pattern obtained below the Curie temperature. However, they found that the spins at the special positions $(0, 0, 0)$ and $(0, 0, 1/2)$ were canted with an angle of 27(8)° with respect to one another. The difference between this canted ferromagnetic structure and our fully ferromagnetic structure could be caused by the Ag doping of our sample, which helps stabilize the perovskite structure and thus results in straighter Mn-O-Mn bond angles. We find

a bond angle of 164.01(4)° for our $La_{0.85}Ag_{0.15}MnO_{3.00+0.10(2)}$ sample, while Alonso *et al.* determined an angle of 163.48(1)° for their $LaMnO_{3+0.15}$ sample [39]. They also investigated a $LaMnO_{3+0.26}$ sample with a bond angle of 165.26(1)°, which unfortunately gave too weak a magnetic signal to make a refinement of the canting angle possible.

An important difference between our LAM sample and the oxygenated LMO samples of Ref. 27 is the amount of holes compared to the amount of vacancies. In Ref. 27, the Mn^{3+}/Mn^{4+} ratio is varied via the oxygen content. Extra oxygen atoms can help facilitate ferromagnetic behaviour because they introduce more holes and straighten out the Mn-O-Mn bond angles as favoured by double exchange. However, a high oxygen content directly correlates with a high amount of vacancies on the Mn site, which will eventually impede collective ferromagnetic exchange. In our sample, holes are introduced via extra oxygen atoms *and* Ag doping, the latter of which does not induce vacancies. It is therefore expected that our sample expresses stronger ferromagnetic behaviour, which may explain why we observe a full ferromagnetic structure with no canting.

A full magnetic Rietveld refinement of the 4 K LAM pattern is shown in the right column of Fig. 2. The refinement has been performed with a nuclear $R\bar{3}c$ phase, a nuclear *Pnma* phase, and the determined ferromagnetic $R\bar{3}c$ phase with spins in the basal plane. The results of the magnetic LAM refinement are also listed in Table 1. The refinement results in a magnetic moment of 3.37(5) μ_B, which agrees rather well with the 3.28(4) μ_B determined from our magnetization data. A phase fraction of 95.02(47)% $R\bar{3}c$ and 4.98(22)% *Pnma* has been identified, confirming that the phase fraction is independent of temperature within error bars (c.f. Fig. 5).

4. Conclusions

Neutron powder diffraction has been employed to study the $La_{0.85}Ag_{0.15}MnO_{3+\delta}$, $\delta = 0.10(2)$, (LAM) manganite perovskite in order to establish its magnetic and structural properties. At room temperature we identify a dominant rhombohedral structure with a space group of $R\bar{3}c$. Below the Curie temperature of $T_c = 246$ K, we observe the same structural $R\bar{3}c$ phase and a ferromagnetic structure with spins oriented perpendicular to the long c-axis.

Our neutron scattering data shows no indication of canting behaviour, which has otherwise been observed in other rhombohedral lanthanum manganites with an excess amount of oxygen. We believe that the lack of canting is a result of the Ag doping, which introduces holes to the compound without also introducing vacancies. The lack of any canting results in a larger sample magnetization, M, and therefore a larger change in M with T close to T_c, and hence a larger entropy change and magnetocaloric effect. Our study underscores the general applicability of monovalent ions as dopants that can be used to tune the magnetic structure of magnetocaloric manganites.

Acknowledgements

We gratefully acknowledge the Science and Technology Facilities Council (STFC) for access to neutron beamtime allocation at the ISIS pulsed Neutron and Muon Source. This work was partially supported by the Çukurova University under project no. FEF2010D11.

References

[1] M.-H. Phan, S.-C. Yu, Review of the magnetocaloric effect in manganite materials, J. Magn. Magn. Mater. 308 (2007) 325.

[2] V. P. S. Awana, R. Tripathi, N. Kumar, H. Kishan, G. L. Bhalla, R. Zeng, L. S. S. Chandra, V. Ganesan, H. U. Habermeier, Magnetotransport of $La_{0.7}Ca_{0.3-x}Sr_xMnO_3$(Ag): A potential room temperature bolometer and magnetic sensor, J. Appl. Phys. 107 (2010) 09D723.

[3] T. Hashimoto, S. Ishibashi, K. Terakura, Jahn-Teller distortion and magnetic structure in $LaMnO_3$: A first-principles theoretical study with full structure optimizations, Phys. Rev. B 82 (2010) 045124.

[4] E. Pavarini, E. Koch, Origin of Jahn-Teller Distortion and Orbital Order in $LaMnO_3$, Phys. Rev. Lett. 104 (2010) 086402.

[5] P. Rivero, V. Meunier, W. Shelton, Electronic, structural, and magnetic properties of $LaMnO_3$ phase transition at high temperature, Phys. Rev. B 93 (2016) 024111.

[6] J. Rodríguez-Carvajal, M. Hennion, F. Moussa, A. H. Moudden, L. Pinsard, A. Revcolevschi, Neutron-diffraction study of the Jahn-Teller transition in stoichiometric $LaMnO_3$, Phys. Rev. B 57 (1998) R3189.

[7] X. Qiu, Th. Proffen, J. F. Mitchell, S. J. L. Billinge, Orbital Correlations in the Pseudocubic O and Rhombohedral R Phases of $LaMnO_3$, Phys. Rev. Lett. 94 (2005) 177203.

[8] C. Zener, Interaction Between the d Shells in the Transition Metals, Phys. Rev. 81 (1951) 440.

[9] L. P. Gor'kov, V. Z. Kresin, Mixed-valence manganites: fundamentals and main properties, Phys. Rep. 400 (2004) 149.

[10] D. N. Argyriou, C. D. Ling, Colossal magnetoresistive manganites, Kluwer Academic Publishers, Dordrecht, The Netherlands, 2004.

[11] V. M. Goldschmidt, Geochemistry, Clarendon Press, Oxford, 1954.

[12] P. G. Radaelli, M. Marezio, H. Y. Hwang, S.-W. Cheong, Structural Phase Diagram of Perovskite $A_{0.7}A'_{0.3}MnO_3$ (A= La, Pr; A′= Ca, Sr, Ba): A New Imma Allotype, J. Solid State Chem. 122 (1996) 444.

[13] H. Y. Hwang, S.-W. Cheong, P. G. Radaelli, M. Marezio, B. Batlogg, Lattice Effects on the Magnetoresistance in Doped $LaMnO_3$, Phys. Rev. Lett. 75 (1995) 914.

[14] A. R. Dinesen, S. Linderoth, S. Mørup, Direct and indirect measurement of the magnetocaloric effect in a $La_{0.6}Ca_{0.4}MnO_3$ ceramic perovskite, J. Magn. Magn. Mater. 253 (2002) 28.

[15] Y. Kalyana Lakshmi, P. Venugopal Reddy, Influence of silver doping on the electrical and magnetic behavior of $La_{0.7}Ca_{0.3}MnO_3$ manganites, Solid State Sci. 12 (2010) 1731.

[16] A. Urushibara, Y. Moritomo, T. Arima, A. Asamitsu, G. Kido, Y. Tokura, Insulator-metal transition and giant magnetoresistance in $La_{1-x}Sr_xMnO_3$, Phys. Rev. B 51 (1995) 14103.

[17] D. Khomskii, Phase separation, percolation and giant isotope effect in manganites, Physica B Condens. Matter 280 (2000) 325.

[18] M. Deutsch, W. Peng, P. Foury-Leylekian, V. Balédent, S. Chattopadhyay, M. T. Fernandez-Diaz, T. C. Hansen, A. Forget, D. Colson, M. Greenblatt, M.-B. Lepetit, S. Petit, I. Mirebeau, Pressure-induced commensurate order in $TbMn_2O_5$ and $DyMn_2O_5$: Influence of rare-earth anisotropy and $3d-4f$ exchange, Phys. Rev. B 98 (2018) 024408.

[19] A. G. Gamzatov, I. K. Kamilov, M. N. Markelova, A. A. Mukhuchev, A. Sh. Asvarov, Resistivity and magnetocaloric effect in manganites $La_{0.75}Ag_{0.125}MnO_{2.85}$ and $La_{0.7}Ag_{0.15}MnO_{2.80}$, Low Temp. Phys. 39 (2013) 953.

[20] I. K. Kamilov, A. G. Gamzatov, A. M. Aliev, A. B. Batdalov, A. A. Aliverdiev, Sh. B. Abdulvagidov, O. V. Melnikov, O. Yu. Gorbenko, A. R. Kaul, Magnetocaloric effect in $La_{1-x}Ag_yMnO_3$ ($y \leq x$): direct and indirect measurements, J. Phys. D 40 (2007) 4413.

[21] A. O. Ayaş and M. Akyol and A. Ekicibil, Structural and magnetic properties with large reversible magnetocaloric effect in

$(La_{1-x}Pr_x)_{0.85}Ag_{0.15}MnO_3$ ($0.0 \leq x \leq 0.5$) compounds, Philos. Mag. 96 (2016) 922.

[22] O. Yu. Gorbenko, O. V. Melnikov, A. R. Kaul, A. M. Balagurov, S. N. Bushmeleva, L. I. Koroleva, R. V. Demin, Solid solutions $La_{1-x}Ag_yMnO_{3+\delta}$: evidence for silver doping, structure and properties, Mater. Sci. Eng. B 116 (2005) 64.

[23] B. Samantaray, S. K. Srivastava, S. Ravi, I. Dhiman, A. Das, Neutron Powder Diffraction Study in $La_{0.85}Ag_{0.15}MnO_3$, J. Supercond. Novel Magn. 24 (2011) 1933.

[24] B. C. Tofield, W. R. Scott, Oxidative nonstoichiometry in perovskites, an experimental survey; the defect structure of an oxidized lanthanum manganite by powder neutron diffraction, J. Solid State Chem. 10 (1974) 183.

[25] A. Wold, R. J. Arnott, Preparation and crystallographic properties of the systems $LaMn_{1-x}Mn_xO_{3+\lambda}$ and $LaMn_{1-x}Ni_xO_{3+\lambda}$ JA-1106, J. Phys. Chem. Solids 9 (1959) 176.

[26] J. A. M. V. Roosmalen, E. H. P. Cordfunke, R. B. Helmholdt, H. W. Zandbergen, The Defect Chemistry of $LaMnO_{3\pm\delta}$: 2. Structural Aspects of $LaMnO_{3\pm\delta}$, J. Solid State Chem. 110 (1994) 100.

[27] J. A. Alonso, M. J. Martínez-Lope, M. T. Casáis, J. L. Macmanus-Driscoll, P. S. I. P. N. de Silva, L. F. Cohen, M. T. Fernández-Díaz, Non-stoichiometry, structural defects and properties of $LaMnO_{3+\delta}$ with high δ values ($0.11 \leq \delta \leq 0.29$), J. Mater. Chem. 7 (1997) 2139.

[28] A. O. Ayaş, M. Akyol, S. K. Çetin, G. Akça, A. Ekicibil, B. Özçelik, Magnetocaloric Properties of $La_{0.85}Ag_{0.15}MnO_3$ and $(La_{0.80}Pr_{0.20})_{0.85}Ag_{0.15}MnO_3$ Compounds, J. Supercond. Novel Magn. 28 (2015) 1649.

[29] R. M. Ibberson, Design and performance of the new supermirror guide on HRPD at ISIS, Nucl. Instr. Methods A 600 (2009) 47.

[30] M. Laver *et al.*, Magnetic structure of magnetocaloric manganites, RB 1610436, STFC ISIS Neutron and Muon Source, https://doi.org/10.5286/ISIS.E.79114884, 2016.

[31] O. Arnold, J. C. Bilheux, J. M. Borreguero, A. Buts, S. I. Campbell, L. Chapon, M. Doucet, N. Draper, R. F. Leal, M. A. Gigg, V. E. Lynch, A. Markvardsen, D. J. Mikkelson, R. L. Mikkelson, R. Miller, K. Palmen, P. Parker, G. Passos, T. G. Perring, P. F. Peterson, S. Ren, M. A. Reuter, A. T. Savici, J. Taylor, R. Taylor, R. Tolchenov, W. Zhou, J. Zikovsky, Mantid - Data analysis and visualization package for neutron scattering and μSR experiments, Nucl. Instr. Methods A 764 (2014) 156.

[32] J. Rodríguez-Carvajal, Recent advances in magnetic structure determination by neutron powder diffraction, Physica B: Condensed Matter 192 (1993) 55.

[33] A. S. Wills, A new protocol for the determination of magnetic structures using simulated annealing and representational analysis (SARAh), Physica B: Condensed Matter 276-278 (2000) 680.

[34] K. Momma, F. Izumi, *VESTA3* for three-dimensional visualization of crystal, volumetric and morphology data, J. Appl. Crystallogr. 44 (2011) 1272.

[35] Q. Huang, A. Santoro, J. W. Lynn, R. W. Erwin, J. A. Borchers, J. L. Peng, R. L. Greene, Structure and magnetic order in undoped lanthanum manganite, Phys. Rev. B 55 (1997) 14987.

[36] B. Chardon, F. Vigneron, Mn_3O_4 commensurate and incommensurate magnetic structures, J. Magn. Magn. Mater. 58 (1986) 128.

[37] G. B. Jensen, O. V. Nielsen, The magnetic structure of Mn_3O_4 Hausmannite between 4.7K and Neel point, 41K, Journal of Physics C: Solid State Physics 7 (1974) 409.

[38] S. Calder, M. D. Lumsden, V. O. Garlea, J. W. Kim, Y. G. Shi, H. L. Feng, K. Yamaura, A. D. Christianson, Magnetic structure determination of Ca_3LiOsO_6 using neutron and x-ray scattering, Phys. Rev. B 86 (2012) 054403.

[39] J. A. Alonso, M. J. Martínez-Lope, M. T. Casáis, A. Muñoz, Magnetic structures of $LaMnO_{3+\delta}$ perovskites (δ = 0.11, 0.15, 0.26), Solid State Commun. 102 (1997) 7.